Supplemental Information

Figure S1. Related to Figure 1.

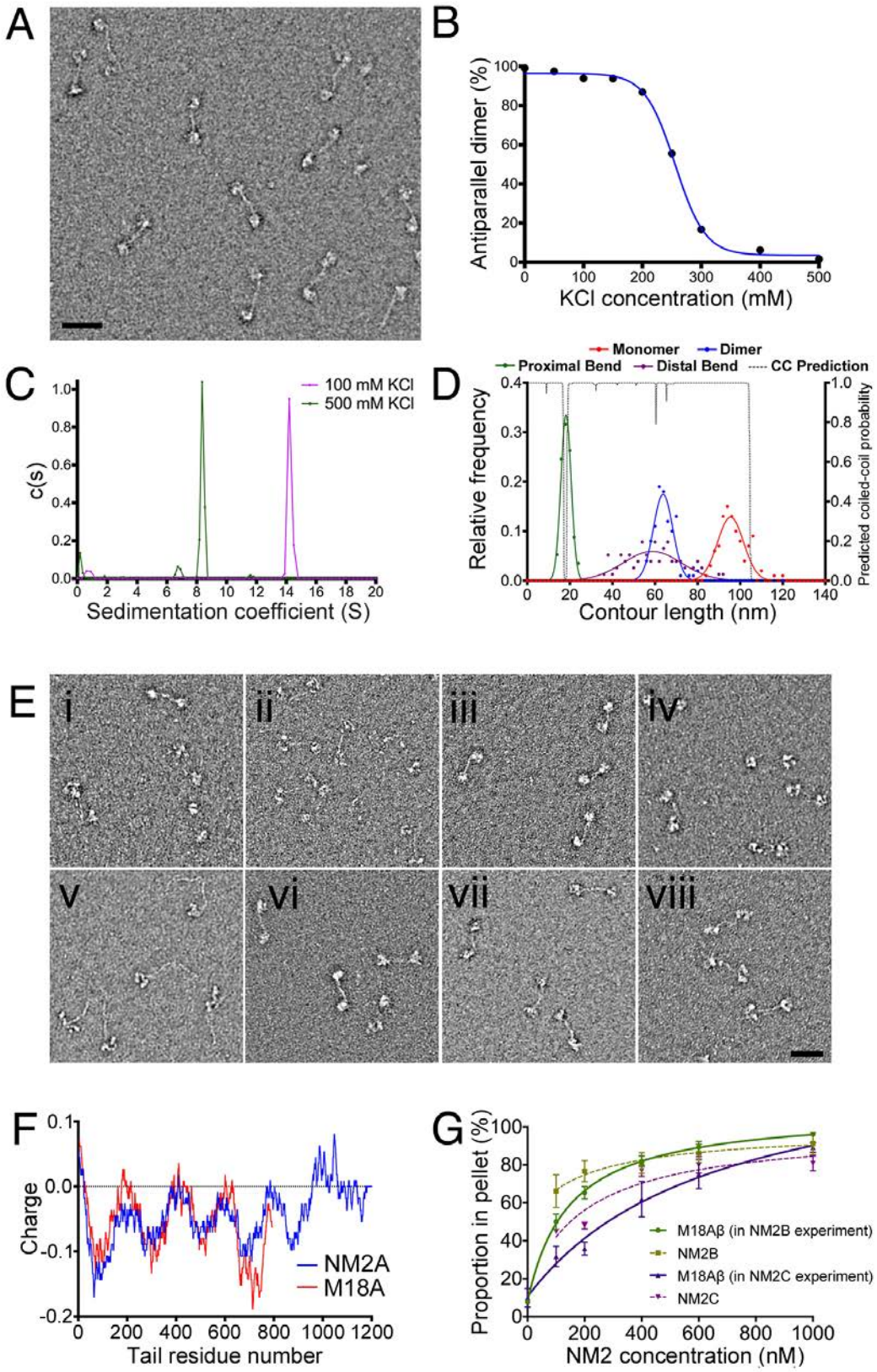

(A) Field of view showing a preparation of M18Aβ in buffer containing 150 mM KCl negatively stained with 1% uranyl acetate (scale bar represents 50 nm). The majority of the molecules are dimeric. (B) Effect of varying salt concentration on the monomer-dimer equilibrium. At KCl concentrations below 255 mM, the majority of molecules are dimers, and at physiological ionic strength (~150 mM) more than 90% of molecules are dimeric. (C) Analytical ultracentrifugation data showing size distribution of M18Aβ in high (500 mM KCl) and low (100 mM KCl) salt buffer. (D) Plot showing contour length distributions for M18Aβ monomers (red) and dimers (blue). Measured bend positions in the tail of the monomer are shown (contour length from the head tail junction to the bend). The most commonly observed and consistent bend position (shown in green) is around 18 nm from the head-tail junction and correlates well with predicted breaks in the coiled-coil (black dotted line). Subsequent bend positions (purple) are variable with the center of the distribution around 59 nm from the head-tail junction. (E) EM images of M18Aβ in various conditions. The scale bar represents 50 nm and applies to all panels. i. Buffer A (10 mM MOPS, 2 mM $MgCl_2$, 0.1 mM EGTA, pH 7.0). ii. Buffer A + 150 mM KCl + 2 mM $CaCl_2$. iii. Tris EDTA buffer (10 mM Tris, 1mM EDTA pH 8.0). iv. Buffer A + 150 mM KCl + 1 mM ADP. v. Buffer A +500 mM KCl. vi. Buffer A + 10 mM $MgCl_2$. vii. Buffer A + 150 mM KCl + 1 mM ATP. viii. Following RLC phosphorylation (Buffer A + 150 mM KCl + 1 mM ATP + 0.2 mM $CaCl_2$ + 1 μM calmodulin + 10 μg/ml MLCK, 60 minute incubation). In all cases except for high ionic strength, M18Aβ forms the bipolar dimer. Filaments were not observed in any condition. (F) Comparison of charge periodicity in the tails of M18A and NM2A. The coiled-coil tail of M18A retains the 196-residue repeat previously documented in class 2 myosins. (G) Cosedimentation of a fixed concentration of M18Aβ (200 nM) with a range of NM2B or NM2C concentrations. Error bars denote S.D.

Figure S2. Related to Figure 2.

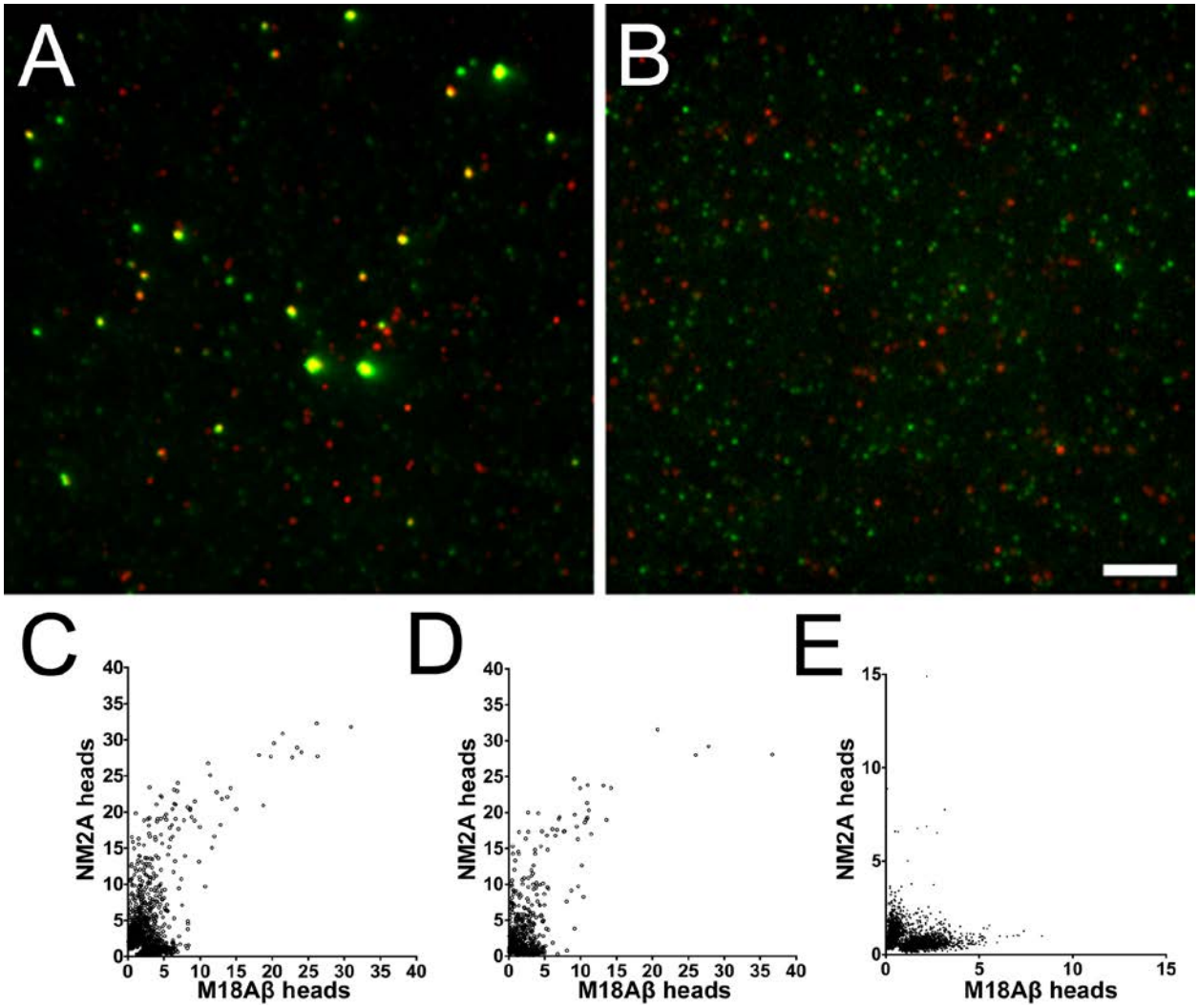

(A) TIRF images of an equimolar mixture of TMR-labelled M18Aβ (red) and Alexa-Fluor 488-labelled NM2A (green) under conditions where the RLCs of both myosins are phosphorylated (Buffer A + 150 mM KCl + 1 mM ATP + 0.2 mM $CaCl_2$ + 1 μM calmodulin + 10 μg/ml MLCK, 60 minute incubation). The image is similar to the one shown in Figure 2A, with clear colocalization of the two myosins in large puncta.

(B) Colocalization of the two myosins is absent in Buffer A + 500 mM KCl , demonstrating that copolymerization is ionic strength dependent. The scale bar represents 2 μm and applies to all panels.

(C) Quantification of the numbers of each myosin in puncta from TIRF fields of equimolar mixtures of unphosphorylated NM2A and M18Aβ in nucleotide free, low salt (150 mM KCl) conditions (as in Figure 2A). (D) Quantification of the numbers of each myosin in puncta from TIRF fields of equimolar mixtures of NM2A and M18A in ATP, following RLC phosphorylation (as in Figure S2B). (E) Quantification of the numbers of each myosin in puncta from TIRF fields of equimolar mixtures of NM2A and M18Aβ in high salt (500 mM KCl) conditions (as in Figure 2C).

Figure S3. Related to Figure 3.

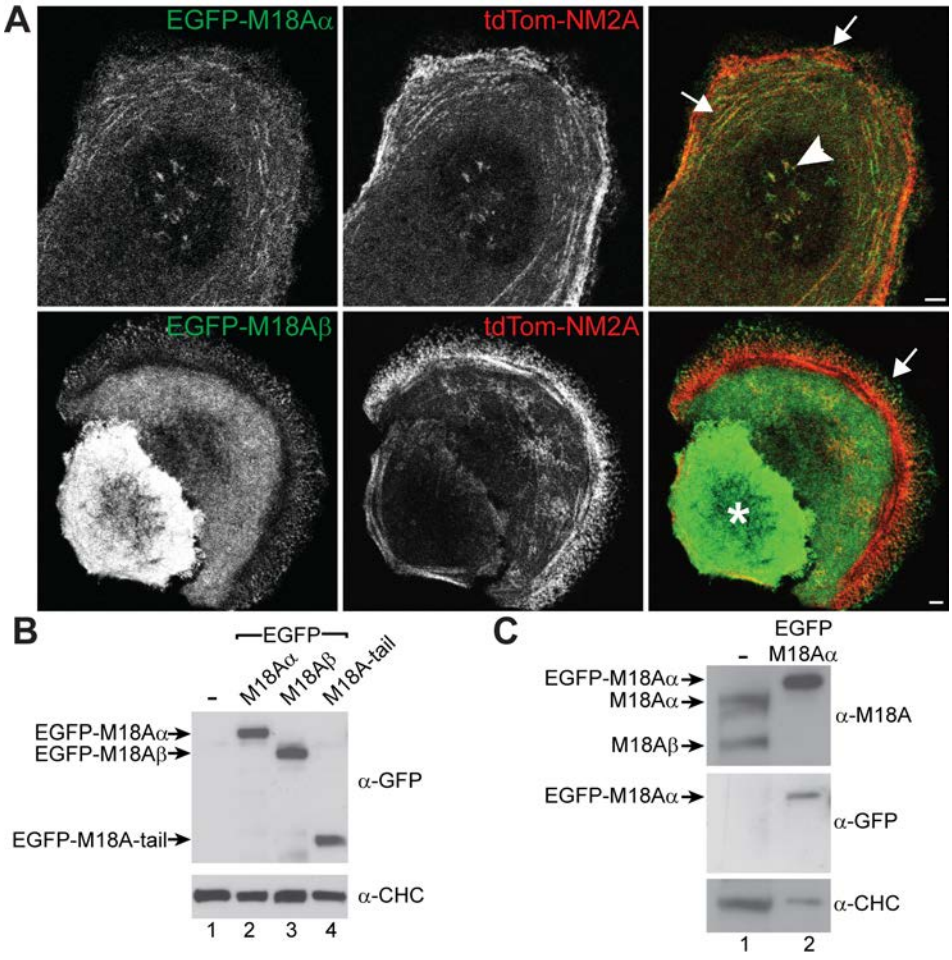

(A) U2OS cells expressing tdTom-NM2A and either EGFP-M18Aα (top row) or EGFP-M18Aβ (bottom row) and were imaged with confocal microscopy. Shown is a single confocal section at the basal surface. Both EGFP-M18Aα and EGFP-M18Aβ localize with tdTom-NM2A in lamellar protrusions (white arrows), with EGFP-M18Aα and tdTom-NM2A also localizing to subnuclear stress fibers (white arrowhead). Note the highly expressing cell in the bottom row (white asterisk) in which EGFP-M18Aβ appears very diffuse. Such diffuse localization was common regardless of cell type when either M18A isoform was highly expressed and precluded the use of such cells for imaging. Scale bars represent 3 μm.

(B) HeLa cells were untransfected (lane 1) or transfected with EGFP-M18Aα, EGFP-M18Aβ, or EGFP-M18A-tail (lanes 2-4, respectively). Whole-cell lysates were collected and subjected to Western blot analysis with the indicated antibody. Because EGFP-M18Aβ is similar in size to endogenous M18Aα, and all EGFP-M18A constructs appear to express at similar levels, EGFP-M18Aα was used for the additional expression analysis in Figure S3C.

(C) HeLa cells were untransfected (lane 1) or transfected with EGFP-M18Aα (lane 2). Whole-cell lysates were collected and subjected to Western blot analysis with the indicated antibody. The sample for lane 2 was diluted to more accurately compare intensities. When normalized for loading and transfection efficiency, the ratio of EGFP-M18Aα to endogenous M18A was 59.2 $\pm$ 8.6 (mean $\pm$ SEM; n = 3). Given the issues with mid to high expressing cells (see above), we typically imaged the lower third of expressing cells with respect to overall fluorescence intensity. Therefore, the degree of over-expression in the cells we imaged was likely closer to ~20 to 25-fold, rather than the ~60-fold over-expression obtained from westerns on all of the cells. Given that the ratio of endogenous M18A to NM2 is ~1:200 ([S5] and data not shown), M18A is still roughly 5-10 fold less abundant than NM2 in over-expressing cells.

Figure S4 Related to Figure 3

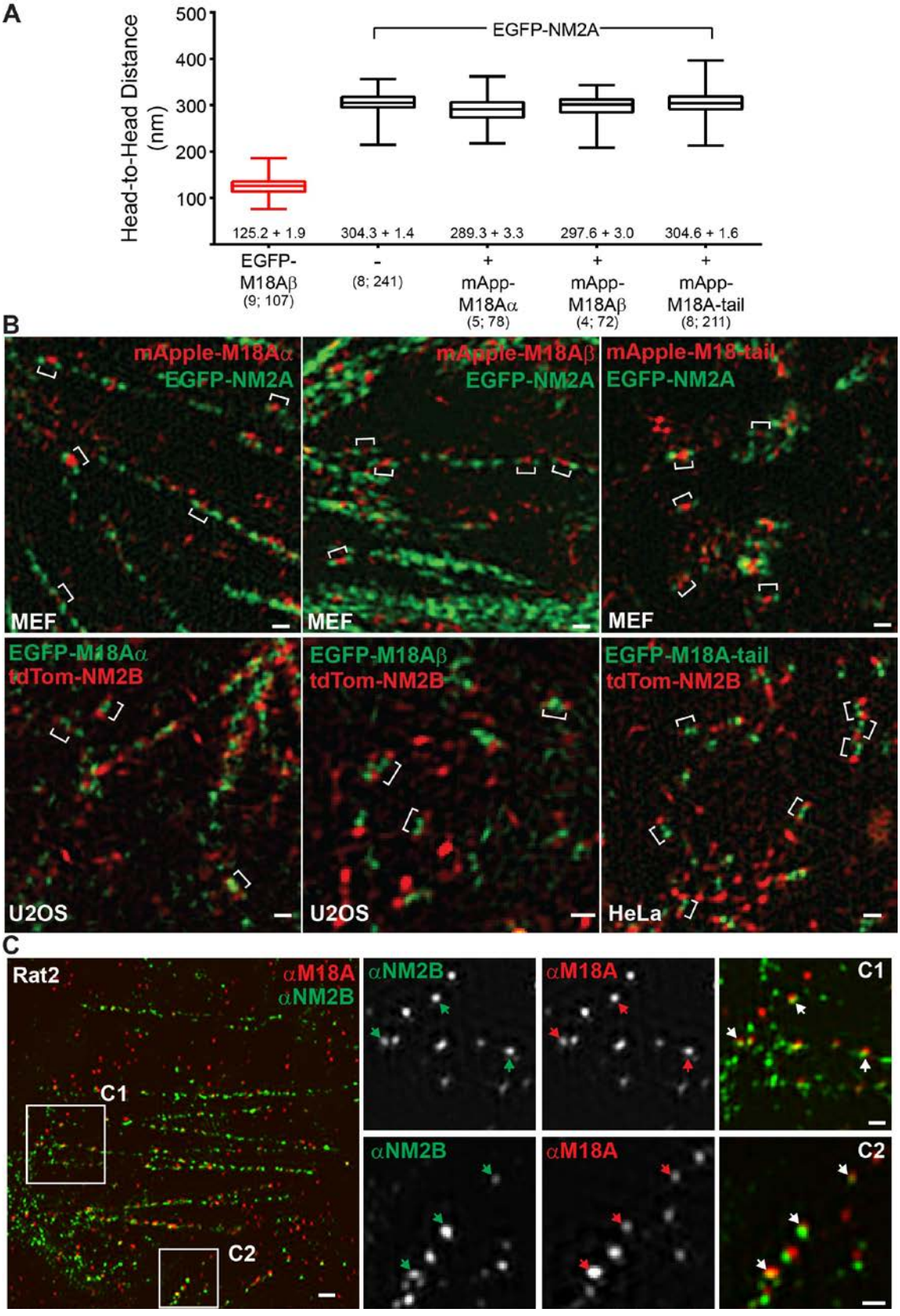

(A) U2OS cells expressing EGFP-M18Aβ and tdTom-NM2A (red plot) or EGFP-NM2A MEFs untransfected or expressing mApple-M18Aα, mApple-M18Aβ, or mApple-M18A-tail (black plots) were imaged with TIRF-SIM. The EGFP centroid was used to measure the head-to-head distance for the indicated myosin when they were in discrete mixed filaments (i.e. filaments of EGFP-M18Aβ were only counted when two discrete EGFP puncta flanked by two red tdTom-NM2A puncta were observed, and filaments of EGFP-NM2A were only counted when two, discrete EGFP puncta were bifurcated by red mApple-M18A puncta). Whiskers indicate min and max. Mean $\pm$ SEM are indicated above the x-axis for each condition. The number of cells used and the number of filaments measured are indicated in parenthesis below each condition. Note that as the measured head-to-head distance for M18Aβ is near the resolution limit for TIRF-SIM, and we are by definition not counting many of the closer head-to-head pairs that do not form discrete puncta, the actual distance may be slightly smaller than indicated. In contrast to our *in vitro* data, we see little or no difference in the head-to-head distance for NM2A when M18Aβ, M18Aα, or the M18A-tail is overexpressed. Given our expression analyses (Figure S3B and S3C), which indicate that M18A remains far sub-stoichiometric to NM2 even when over-expressed (~5 to 10-fold less abundant), the most likely explanation for this discrepancy is that the cellular level of M18A is not sufficiently high to shorten NM2 filaments. It is also possible that there are constraints on filament length when they form *in vivo.* For example, NM2 binding partners may stabilize filament length in cells, or the interaction of filaments with underlying actin structures may minimize filament shortening.

(B) TIRF-SIM imaging reveals coassembly between various combinations of M18Aα, M18Aβ, and the truncated tail of M18A with NM2A and NM2B in different cell types. See the upper portion each image for the fluorophore-tagged myosin constructs being expressed and the lower left corner for the cell type used. White brackets indicate the coassembly of M18A isoforms or the M18A-tail with NM2 isoforms into mixed filaments. Scale bars represent 300 nm.

(C) Rat2 cells immunostained for endogenous M18A (followed by a red secondary antibody) and NM2B (followed by a green secondary antibody) were imaged with TIRF-SIM. The numbered boxes correspond to the row of images to the right, which present grayscale images for M18A and NM2B and the merged image. Arrowheads indicate some of the overlapping green and red puncta indicative of mixed filaments. Note that yellow in the overlay channel is only very obvious when the intensities for red and green are approximately equal, which is often not the case when examining the split images (where commonly the color for NM2 is strong and the color for an overlapping M18A puncta is not). Scale bars represent 2 μm for the larger image and 300 nm for insets.

Supplemental Experimental Procedures

Sequence analyses — Coiled-coil prediction for M18A was conducted using the COILS server, with a window size of 28 residues (http://embnet.vital-it.ch/software/COILS_form.html) [S1]. Analyses of charge distribution in myosin tails were carried out using a modified version of BH-search (http://helixweb.nih.gov/bhsearch/). Aspartic and glutamic acid residues were assigned a value of -1, arginine and lysine residues were assigned a value of +1, and all other residues were assigned a value of 0. Additional residues with a value of 0 were added to the C-terminus of the sequence to allow averaging over a large window. Charge was calculated based on the average within a window of 112 residues centered on the specified residue. The starting residue for the tails of both M18A and NM2A was taken as the first residue after the head tail junction (i.e. the post-proline residue in the sequences VRPLIQ and VKPLLQ for M18A and NM2A, respectively). Charge was calculated for the entire tail region beyond this point.

Analytical ultracentrifugation — M18A was centrifuged in a buffer containing 10 mM MOPS, 0.1 mM EGTA, and 1 mM TCEP and either 100 mM KCl or 500 mM KCl, as stated in the text. Sedimentation velocity experiments were performed at 20 °C, 32000 RPM using a ProteomeLab XL-I analytical ultracentrifuge (Beckman Coulter, Brea, CA) and absorption detection optics. Data were analyzed using Sedfit software with partial specific volumes calculated from sequence, and buffer composition by the Sednterp program [S2].

Mammalian expression vectors — Plasmids EGFP-M18Aα and EGFP-M18Aβ were created by inserting the previously published sequences for *Mus musculus* M18Aα and M18Aβ [S1] into pEGFP-C1 (Clontech). Plasmid EGFP-M18A-tail was created by cloning the C-terminal 795 residues of M18A (Pro-1240 to the stop codon) into pEGFP-C1. Plasmids mApple-M18Aa, mApple-M18Ab, and mApple-M18A-tail were then created by replacing the EGFP with mApple. Plasmid tdTomato-NM2A was

created by substituting the td-Tomato fluorophore for the EGFP fluorophore in EGFP-C3-NM2A (Addgene #11347). Plasmid tdTomato-NM2B was a gift from the Waterman lab (NHLBI). All plasmids were created using standard molecular biological techniques and were sequence verified.

Cell culture and transfection — HeLa, Rat2, MEF, and U2OS cells were maintained in Dulbecco's modified Eagle's medium supplemented with 10% fetal bovine serum, 2 mM GlutaMAX (Life Technologies, Grand Island, NY), and 1X antibiotic-antimycotic (Life Technologies). Cells were maintained at 37°C in 5% CO_2. MEF cells were isolated from EGFP-NM2A knock-in mice [S3] as previously described [S4]. All coverslips were coated with 10 μg/ml fibronectin (Sigma, St. Louis, MO) prior to use. Cells were transfected using the Lonza Nucleofector system as described previously for U2OS cells [S5].

Head-to-Head analysis — For measurement of the head-to-head distance of M18A, U2OS cells expressing EGFP-M18Aβ and tdTom-NM2A were imaged with TIRF-SIM. For measurement of head-to-head distance of NM2A, EGFP-NM2A knock-in MEFs expressing mApple-M18Aα, mApple-M18Aβ, or mApple-M18A-tail were imaged with TIRF-SIM. The EGFP centroid was used to measure head-to-head distance for the indicated myosin when they were in discrete mixed filaments (i.e. filaments of EGFP-M18Aβ were only counted when two discrete EGFP puncta flanked by two red tdTom-NM2A puncta were observed, and filaments of EGFP-NM2A were only counted when two discrete EGFP puncta were bifurcated by red mApple-M18A puncta). Puncta centroids were localized using ImageJ.

Reference List

S1. Lupas A., Van D.M., and Stock J. (1991). Predicting coiled coils from protein sequences. Science *252*: 1162-1164.

S2. Lebowitz J., Lewis M.S., and Schuck P. (2002). Modern analytical ultracentrifugation in protein science: a tutorial review. Protein Sci *11*: 2067-2079.

S3. Zhang Y., Conti M.A., Malide D., Dong F., Wang A., Shmist Y.A., Liu C., Zerfas P., Daniels M.P., Chan C.C. et al. (2012). Mouse models of MYH9-related disease: mutations in nonmuscle myosin II-A. Blood *119*: 238-250.

S4. Bockholt S.M. and Burridge K. (1995). An examination of focal adhesion formation and tyrosine phosphorylation in fibroblasts isolated from src-, fyn-, and yes- mice. Cell Adhes. Commun. *3*: 91-100.

S5. Beach J.R., Shao L., Remmert K., Li D., Betzig E., and Hammer J.A., III (2014). Nonmuscle myosin II isoforms coassemble in living cells. Curr. Biol *24*: 1160-1166.